Laminar-turbulent transition for low Reynolds number mixed convection in a uniformly heated vertical tube

Received November 2001
Accepted June 2002

A. Behzadmehr, N. Galanis and A. Laneville
Génie Mécanique, Université de Sherbrooke, Sherbrooke, QC, Canada

Keywords *Convection, Tube, Numerical methods*

Abstract *Upward mixed convection flow of air in a uniformly heated vertical tube was studied numerically using the three-dimensional elliptic conservation equations and the Launder and Sharma low Reynolds number* $k-\varepsilon$ *turbulence model. For* $\mathrm{Re} = 1,000$ *the fully developed flow field undergoes two transitions as the Grashof number increases: thus, this flow field is laminar for* $Gr < 8 \times 10^6$*, turbulent for* $8\times10^6 < Gr < 5 \times 10^7$ *and again laminar for* $Gr > 5 \times 10^7$*. In the entry region, turbulent kinetic energy decays monotonically for* $Gr \leq 3 \times 10^6$ *and* $Gr \geq 7.1 \times 10^7$*. For Gr between these two values it initially increases from the imposed inlet condition and then decreases towards its calculated fully developed value. The mean velocity profiles as well as the axial evolution of the skin friction coefficient are presented for representative values of Gr.*

Nomenclature

D = Internal tube diameter
C_f = Skin friction coefficient ($=2\tau_w/\rho U_0^2$)
C_p = Specific heat
G = Turbulent production
g = Acceleration of gravity
Gr = Grashof number ($=g\beta D^4 q_w/\lambda\nu^2$)
I = Turbulent intensity
k = Turbulent kinetic energy
P = Time mean pressure
Pr = Prandtl number($=\mu C_p/\lambda$)
q_w = Uniform heat flux at the solid–fluid interface
r = Radial coordinate
Re = Reynolds number ($=U_0 D/\nu$)
T, t = Time mean and fluctuating temperature
U, u = Time mean and fluctuating velocity
Z = Axial coordinate

Greek letters
β = Volumetric expansion coefficient
ε = Dissipation of turbulent kinetic energy
θ = Tangential coordinate
λ = Thermal conductivity
μ = Dynamic viscosity
ν = Kinematic viscosity
ρ = Density
τ = Shear stress

Subscripts
B = Bulk
b = Buoyancy

The authors thank the Natural Sciences and Engineering Research Council of Canada for its financial support as well as the Ministry of Science, Research and Technology of the I. R. Iran for the scholarship awarded to the first author.

International Journal of Numerical Methods for Heat & Fluid Flow, Vol. 12 No. 7, 2002, pp. 839-854.

DOI 10.1108/09615530210443052

c = Centerline
i,j = Tensor index
ℓ = Hydrodynamic turbulence production
w = Wall
0 = Inlet condition
r = Radial direction
z = Axial direction
θ = Tangential direction

Introduction

Mixed convection in ducts occurs in many industrial installations such as pressurized water reactors, supercritical boilers, solar energy collectors and shell and tube heat exchangers. Therefore, it is being studied extensively. Jackson *et al.* (1989) presented a comprehensive review of experimental and theoretical studies on mixed convection in vertical tubes published before 1989. Several more recent publications are referred to in the present article.

Numerical studies of mixed convection have been conducted by assuming that the flow field is laminar when Re is low or turbulent when Re is high. Thus, Zeldin and Schmidt (1972), Wang *et al.* (1994) and Ouzzane and Galanis (1999) used the laminar equations for $\mathrm{Re} < 1500$ while Cotton and Jackson (1990), Satake *et al.* (2000) and Tanaka *et al.* (1987) used the turbulent equations for $\mathrm{Re} > 2,000$. Nevertheless, experimental evidence compiled by Metais and Eckert (1964) indicates that mixed convection can be turbulent for Reynolds numbers as low as 1,000. The structure of such very low Reynolds number mixed convection flows has not been studied systematically.

Furthermore, a flow field, which is laminar at the tube entrance, may become unstable and eventually turbulent further downstream or, as demonstrated by both numerical and experimental studies (Hall and Jackson, 1969; Satake *et al.*, 2000; Tanaka *et al.*, 1987) a turbulent flow can become laminar under the stabilizing effect of the buoyancy force. It is, therefore, evident that the laminar model used for the numerical prediction of the corresponding hydrodynamic and thermal fields is of limited practical interest since it can only handle the simplest flow conditions.

In view of these observations, it is preferable to use turbulent models with a proven capability of predicting laminar flow fields for the analysis of convection heat transfer. The low Reynolds number k-ε models are among the primary candidates for such analyses. Indeed, Jones and Launder (1972) have shown that in some cases turbulent solutions for such a model do not exist for accelerating flows. They state, that "if one starts the predictions with an initially turbulent boundary layer and then applies the acceleration, the turbulence gradually decays away and the mean velocity profile collapses to that appropriate to laminar flow". Cotton and Jackson (1990) used a slightly different version of this k-ε model to study the heat developed due to flow in tubes. Their numerical results were calculated with $\mathrm{Re} = 5,000$, $\mathrm{Pr} = 0.7$ and $4.4 \times 10^5 < \mathrm{Gr} < 9.0 \times 10^8$. They are in close agreement with experimental heat transfer data and with flow profile measurements for air. These authors established that the mean flow equations and the turbulence model must be

cast in a developing flow framework in order to capture the complex behavior occurring in ascending heated flows.

In view of this situation, our research on mixed convection in tubes which has until now focused on laminar flow (Ouzzane and Galanis, 1999; Orfi *et al.*, 1999; Nesreddine *et al.*, 1998) is being extended to include turbulent flows. In this paper, the Launder and Sharma (1974) low Reynolds number k-ε model is used to study ascending mixed convection with uniform heating for $\mathrm{Pr} = 0.7$, $\mathrm{Re} = 1,000$ and a wide range of Grashof numbers. Specifically, the aim of this study is to establish the transition conditions between laminar and turbulent flows, and to obtain a comprehensive description of the axial evolution of the hydrodynamic field. Similar numerical investigations of the transitional features of heated flows have dealt with forced convection and Reynolds numbers higher than 2,000 (Ezato *et al.*, 1999; Torii and Wen-Jei, 2000). As far as we can ascertain, this work constitutes the first systematic numerical study of the flow regime evolution for mixed convection with $\mathrm{Re} < 2,000$.

Mathematical formulation and numerical procedure

We consider air flowing upwards in a long vertical tube with uniform heating at the fluid–solid interface. The properties of the air are assumed constant except for the density in the body force which varies linearly with temperature (Boussinesq's hypothesis). Dissipation and pressure work are neglected. With these assumptions the dimensional conservation equations for steady state mean conditions are as follows:

$$\frac{\partial U_j}{\partial X_j} = 0 \tag{1}$$

$$\rho \frac{\partial}{\partial X_j}(U_j U_i) = \frac{-\partial P}{\partial X_i} + \frac{\partial}{\partial X_j}\left[\mu\left(\frac{\partial U_i}{\partial X_j} + \frac{\partial U_j}{\partial X_i}\right) - \rho\overline{u_i u_j}\right] + [1 - \beta(T - T_0)]\ \rho g_i \tag{2}$$

$$\rho \frac{\partial}{\partial X_j}\left(C_\mathrm{p} U_j \frac{\partial T}{\partial X_j}\right) = \frac{\partial}{\partial X_j}\left[\lambda \frac{\partial T}{\partial X_j} - C_\mathrm{p}\rho\overline{u_j t}\right] \tag{3}$$

In cylindrical coordinates:

$$X_1 = r, \qquad X_2 = \theta, \qquad X_3 = Z \tag{4a}$$

For Z positive in the flow direction,

$$g_1 = g_2 = 0 \ \text{ and } \ g_3 = -g. \tag{4b}$$

Turbulence is modeled with the Launder and Sharma (1974) low Reynolds number k-ε model which has been shown (Carr *et al.*, 1973) to give accurate predictions for low and intermediate Reynolds numbers and for boundary

layers with adverse pressure gradients. It has also been successfully used (Cotton and Jackson, 1990) to model turbulent mixed convection for $\mathrm{Re} \geq 2,100$ and is expressed by the following relations for the turbulent kinetic energy and turbulent energy dissipation, respectively:

$$\frac{\partial}{\partial X_j}(U_j k) = \frac{\partial}{\partial X_j}\left[\left(\nu + \frac{\nu_t}{\sigma_k}\right)\frac{\partial k}{\partial X_j}\right] + G_k + G_b - \varepsilon - 2\nu\left(\frac{\partial \sqrt{k}}{\partial X_j}\right)^2 \tag{5}$$

$$\frac{\partial}{\partial X_j}(U_j \varepsilon) = \frac{\partial}{\partial X_j}\left[\left(\nu + \frac{\nu_t}{\sigma_\varepsilon}\right)\frac{\partial \varepsilon}{\partial X_j}\right] + c_1 f_1 \frac{\varepsilon}{k}(G_k + G_b) - c_2 f_2 \frac{\varepsilon^2}{k} + 2\nu\nu_t\left(\frac{\partial^2 U_i}{\partial X_j \partial X_k}\right)^2 \tag{6}$$

where

$$G_k = -\overline{u_i u_j}\frac{\partial U_i}{\partial X_j}, \quad G_b = -\frac{\beta}{\rho} g_i \overline{u_i t} = g_i \frac{\beta}{\rho}\frac{\nu_t}{\mathrm{Pr}_t}\frac{\partial T}{\partial X_i}, \quad \nu_t = c_\mu f_\mu \frac{k^2}{\varepsilon}$$

$$c_1 = 1.44, \quad c_2 = 1.92, \quad c_\mu = 0.09, \quad f_1 = 1, \quad \mathrm{Pr}_t = 0.9, \quad \sigma_k = 1, \quad \sigma_\varepsilon = 1.3$$

$$f_2 = 1 - 0.3\ \exp(-R_t^2), \quad f_\mu = \exp\left[\frac{-3.4}{(1 + R_t/50)^2}\right], \quad R_t = \frac{k^2}{\nu\varepsilon} \tag{7}$$

It should be noted that no assumption of symmetry is introduced, the field variables are then considered to vary with all three space coordinates. These equations have been presented in cylindrical coordinates by Cotton and Jackson (1990) with the boundary layer approximation and by Tanaka *et al.* (1987) for fully developed flows. The model used in the present study does not use either of these simplifications.

The boundary conditions are as follows:

- At the tube entrance ($Z = 0$):

$$U_z = U_0 \qquad U_\theta = U_r = 0 \qquad T = T_0 \qquad I = I_0 \tag{8a}$$

Since the adopted model incorporates the assumption of turbulence isotropy, the corresponding turbulent kinetic energy is:

$$k_0 = 1.5(I_0 U_0)^2 \tag{8b}$$

- At the tube outlet ($Z = 101\mathrm{D}$):

$$\text{All axial derivatives are zero} \tag{9}$$

- At the fluid–solid interface ($r = D/2$):

$$U_r = U_\theta = U_Z = 0, \qquad k = \varepsilon = 0, \qquad q_{\mathrm{w}} = -\lambda \frac{\partial T}{\partial r} \tag{10}$$

This set of coupled non-linear differential equations was discretized with the control volume technique. For the convective and diffusive terms a second order upwind method was used while the SIMPLEC procedure was introduced for the velocity–pressure coupling. The relative convergence criterion is

$$\frac{R^{\phi}_{\text{iteration}\,N}}{R^{\phi}_{\text{iteration}\,M}} < \delta \tag{11}$$

For continuity $R^{\varphi} = \sum |\,\text{rate of mass creation in cell}\,|$ and $\delta = 10^{-3}$. Otherwise, the scaled residual R^{φ} is defined as

$$R^{\varphi} = \frac{\sum_{\text{cell p}} \left| \sum_{\text{nb}} a_{\text{nb}} \phi_{\text{nb}} + b - a_{\text{p}} \phi_{\text{p}} \right|}{\sum_{\text{cell p}} |a_{\text{p}} \phi_p|} \tag{12}$$

where nb indicates the neighbors of cell p. For velocities $\varphi = U_i$ and $\delta = 10^{-3}$, for turbulent kinetic energy $\varphi = k$ and $\delta = 10^{-3,}$ for turbulent dissipation $\varphi = \varepsilon$ and $\delta = 10^{-3}$ while for energy $\varphi = T$ and $\delta = 10^{-6}$.

The discretization grid is uniform in the circumferential direction and non-uniform in the other two directions. It is finer near the tube entrance and near the wall where the velocity and temperature gradients are large. Several different grid distributions have been tested to ensure that the calculated results are grid independent. Although none of these tests showed any variation in the circumferential direction, we retained the three-dimensional formulation for future considerations. The selected grid for the present calculations consisted of 220, 48 and 8 nodes, respectively, in the axial, radial and circumferential directions. Results with (440, 96, 8) nodes differed by 0.5 percent or less for velocity components, temperature, turbulent kinetic energy and turbulent dissipation.

Validation and results

In this section, we present results calculated with the previously presented model, which demonstrate its versatility and illustrate the effect of the Grashof number on the flow regime. The Prandtl number was held constant at 0.7 throughout this study.

a. Validation

In order to demonstrate the validity and precision of the model and the computer code, calculated velocity and temperature profiles have been compared with corresponding experimental results from the literature. Figure 1 shows such a comparison with measurements by Carr *et al.* (1973) corresponding to fully developed turbulent flow. The calculated results were obtained with $I_0 = 8$ percent according to an appropriate empirical relation (Karasu, 1995). The agreement between numerical and experimental values for both the temperature and velocity profiles is very good.

Figure 2 shows similar comparisons with measurements by Zeldin and Schmidt (1972) for developing laminar flow in a vertical isothermal tube. Calculations with $I_0 = 8$ percent and $I_0 = 0.8$ percent resulted in identical results for the velocity and temperature profiles at the axial positions identified in Figure 2. A detailed comparison of the calculated results indicates that for such laminar flow conditions the influence of I_0 on the mean axial velocity and temperature is restricted to the immediate vicinity of the tube entrance. Once again the agreement between numerical and experimental values is very good except for the temperature profile near the tube entrance ($Z/Pe = 0.01496$ or $Z/D \cong 4$). However, as explained by Zeldin and Schmidt (1972) the measured temperatures close to the tube entrance were influenced by upstream conduction through the walls of the experimental setup. The numerical predictions of their laminar model for the temperature profile at $Z/D \cong 4$ are very close to the numerical results in Figure 2.

The results of these two figures demonstrate the validity of the physical model and the numerical procedure for the calculation of both turbulent and laminar flows. Furthermore, they show that in the case of laminar flows the mean velocity and temperature profiles are essentially independent of the upstream turbulent intensity.

b. Axial evolution of the hydrodynamic field

Figure 3 shows the axial evolution of the turbulent kinetic energy for the laminar conditions specified in Figure 2. As the fluid moves downstream, k decreases for all radial positions. The decay of turbulent kinetic energy occurs earlier when the imposed value of I_0 is smaller but the value of k is negligible after a length of approximately 30 D even for the admittedly excessive value of $I_0 = 8$ percent. As mentioned earlier, for such laminar flow conditions the value of I_0 does not influence the distribution of U and T. However, convergence is quicker when I_0 is smaller and it is therefore preferable to use low values of this parameter when laminar flow conditions are suggested by charts such as those by Metais and Eckert (1964). The results of Figures 2 and 3 are consistent with the remark by Jones and Launder (1972) quoted in the introduction.

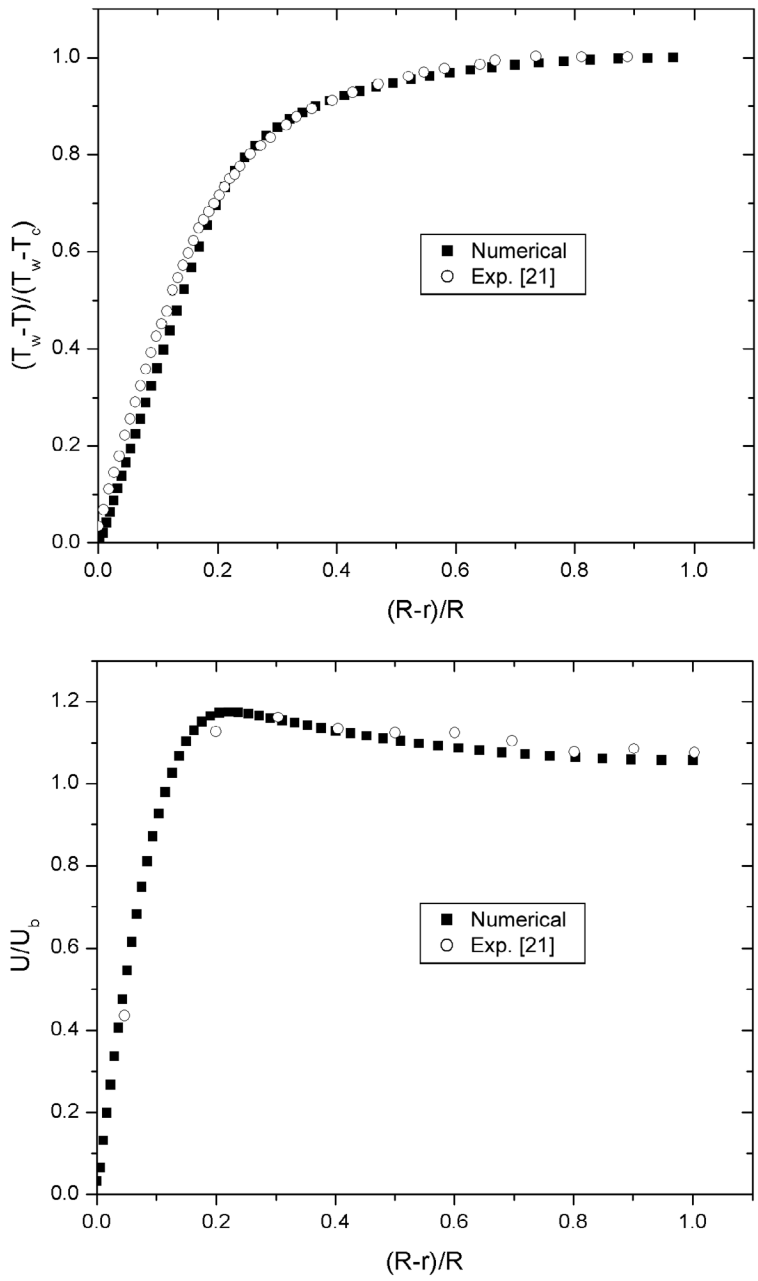

Figure 1.
Validation for turbulent flow conditions ($\mathrm{Pr} = 0.71$, $\mathrm{Re} = 5,000$, $\mathrm{Gr} = 2.22 \times 10^7$, $I_0 = 8$ percent)

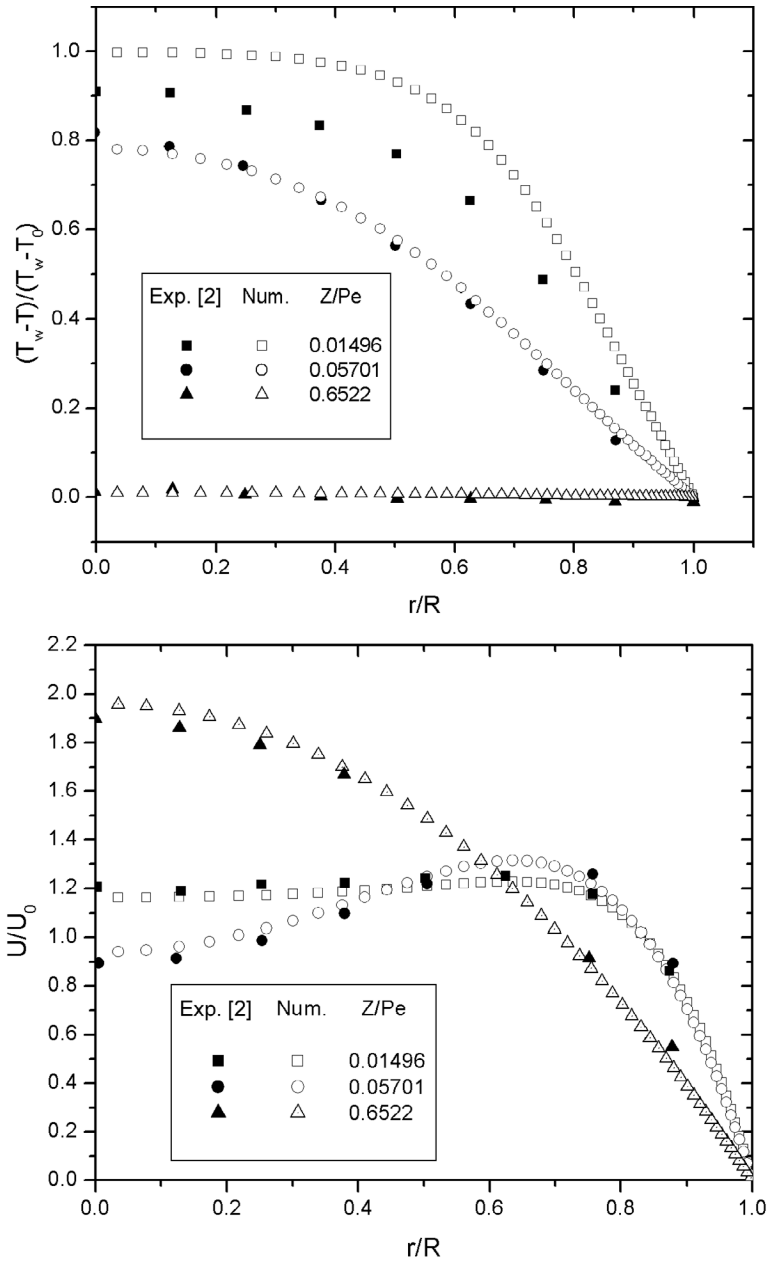

Figure 2.
Validation for laminar flow conditions ($Pr = 0.71$, $Re = 379.8$, $Gr_t = 12,628$, $I_0 = 8$ percent)

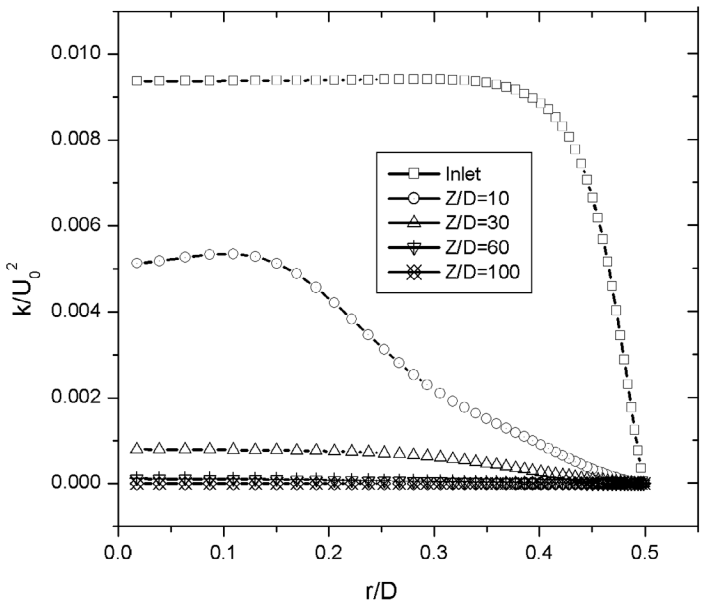

Figure 3.
Evolution of turbulent kinetic energy for laminar flow conditions ($Pr = 0.71$, $Re = 379.8$, $Gr_t = 12,628$, $I_0 = 8$ percent)

The Reynolds number and the entrance turbulent intensity were then fixed at 1,000 and 0.1 percent, respectively, in order to study the effect of the Grashof number on the flow characteristics.

Figure 4 shows the axial evolution of the centerline mean axial velocity U_c for four different Grashof numbers. At the inlet ($Z = 0$) $U_c = U_0$ for all values of Gr. Immediately afterwards, U_c increases as the boundary layer builds up and pushes the fluid towards the tube axis. This effect is counterbalanced by the upward acceleration of the fluid in the vicinity of the wall induced by buoyancy. Thus, eventually U_c reaches a maximum. The position of this maximum approaches the tube entrance as the Grashof number increases. Beyond this position, the fluid velocity in the vicinity of the wall continues to increase and U_c decreases to satisfy continuity. Further downstream however, the behavior of U_c is more complicated. For the lowest Grashof number, $Gr = 7.1 \times 10^5$, it eventually reaches a positive constant value approximately equal to U_0. For $Gr = 4.5 \times 10^6$ it becomes negative, goes through a local minimum and reaches a negative constant value indicating the existence of flow reversal which persists everywhere beyond $Z \cong 12D$. For $Gr = 10^7$ the evolution of U_c is quite different. After the maximum value caused by the boundary layer buildup and the subsequent rapid decrease, it reaches a negative value at approximately $Z = 10D$ and then increases towards a second positive local maximum. Flow reversal in this case is therefore very localized. After the second local maximum and a rapidly damped oscillation it reaches a

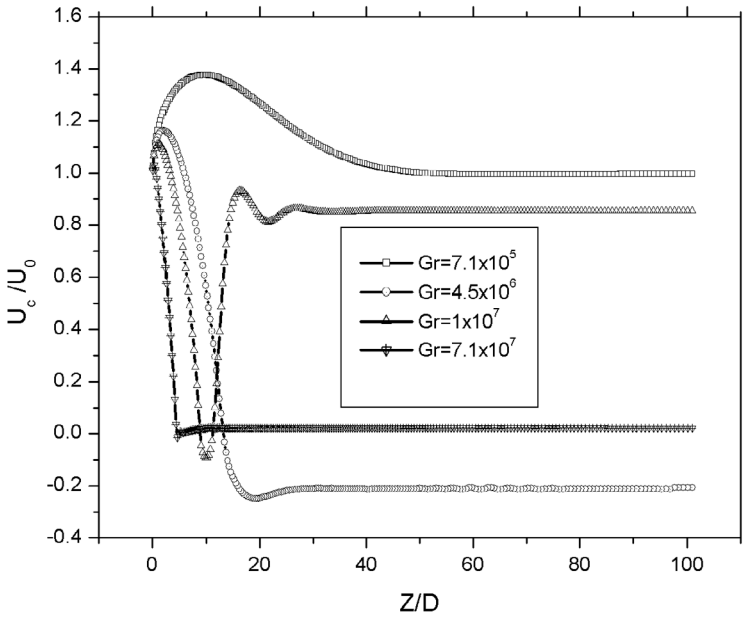

Figure 4.
Evolution of the centerline mean axial velocity (Pr = 0.7, Re = 1,000, $I_0 = 0.1$ percent)

positive constant value approximately equal to $0.85U_0$. Finally, for the highest Grashof number, $\mathrm{Gr} = 7.1 \times 10^7$, the maximum induced by the boundary layer growth is hardly visible. U_c decreases rapidly towards zero, increases slightly and reaches a constant positive value, which is less than $0.05U_0$.

It is important to note that the relation between Gr and the constant value of U_c, whose existence has been established by the results of Figure 4, is not monotonic. Indeed the values of the ratio U_c/U_0 are 1.0, -0.2, 0.85 and 0.03 for Gr equal to 7.1×10^5, 4.5×10^6, 10^7 and 7.1×10^7, respectively. In order to put into perspective and validate this peculiar relation, it is first necessary to establish the turbulent characteristics of each of these four flow fields.

Figure 5 shows the axial evolution of the centerline turbulent kinetic energy for the previously specified four Grashof numbers. Radial distributions of k at different axial positions have also been obtained but are not shown here because of space limitations. In the immediate vicinity of the tube entrance ($Z/D \leq 2$) k_c is identical for all four Grashof numbers (note the difference in scales between the two parts of the figure). Beyond this axial position the evolution of k_c depends very strongly on the Grashof number. For the lowest Grashof number, $\mathrm{Gr} = 7.1 \times 10^5$, turbulence is damped monotonically and laminar conditions prevail in the downstream part of the tube. For $\mathrm{Gr} = 4.5 \times 10^6$, Figure 5 shows a growth of turbulence with a peak value at approximately $Z = 30D$. Once again the flow field in the downstream part of the tube is laminar. As Gr increases further, the flow becomes more unstable

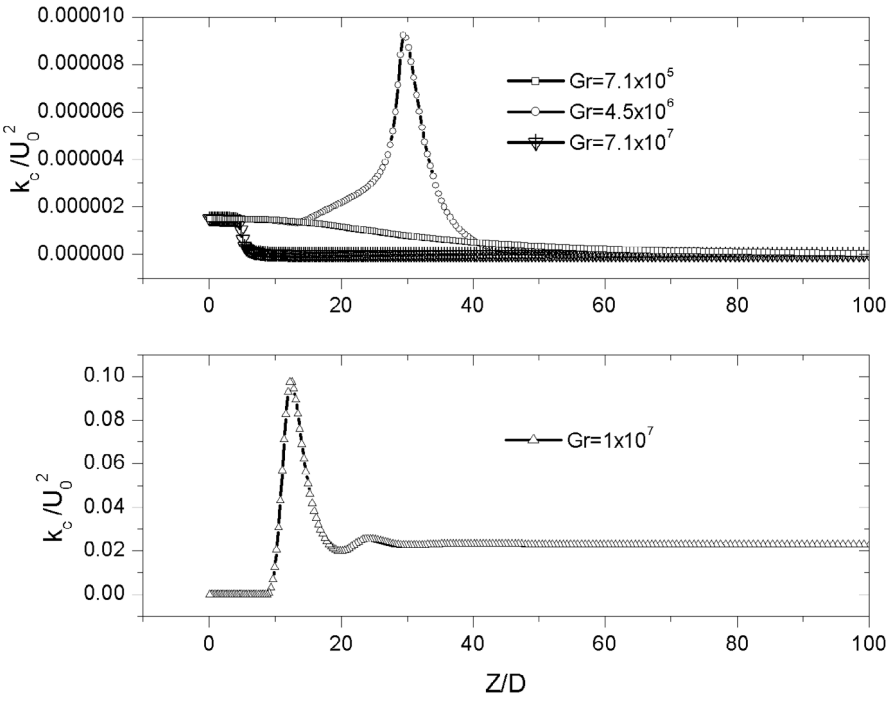

Figure 5.
Evolution of the centerline turbulent kinetic energy ($\mathrm{Pr} = 0.7$, $\mathrm{Re} = 1,000$, $I_0 = 0.1$ percent)

and for $\mathrm{Gr} = 10^7$ it is turbulent everywhere beyond $Z/D \cong 10$ due to the simultaneous increase of buoyancy turbulent production and of turbulent diffusion. Finally, for the highest value, $\mathrm{Gr} = 7.1 \times 10^7$, k_c is uniformly zero beyond $Z/D \cong 5$ due to the laminarization effect of the buoyancy force already reported in the literature (Hall and Jackson, 1969; Satake *et al.*, 2000; Tanaka *et al.*, 1987). The results of Figure 5 shows that, for $\mathrm{Re} = 1000$, the flow field undergoes two transitions as the Grashof number increases: for low Grashof numbers the flow is laminar everywhere, for intermediate Grashof numbers (between approximately 10^6 and 5×10^7) it is turbulent in at least certain parts of the tube while for $\mathrm{Gr} = 7.1 \times 10^7$ it is again laminar. Figure 5 also shows that in the downstream part of the tube k_c is independent of the axial position, similar to U_c.

Figure 6a shows the axial evolution of the mean velocity profile for $\mathrm{Gr} = 10^7$ in the entry region where it undergoes significant changes. It does not include the very short region where U_c increases (cf. Figure 4) due to the boundary layer buildup. It does show, however, that between $Z/D = 6$ and $Z/D = 10$ the velocity near the wall is accelerated due to the influence of buoyancy while the corresponding velocity near the tube axis decreases. This behavior is typical for laminar flows (Wang *et al.*, 1994; Nesreddine *et al.*, 1998) and indeed, as shown in Figure 4, the flow field under consideration is laminar in this region.

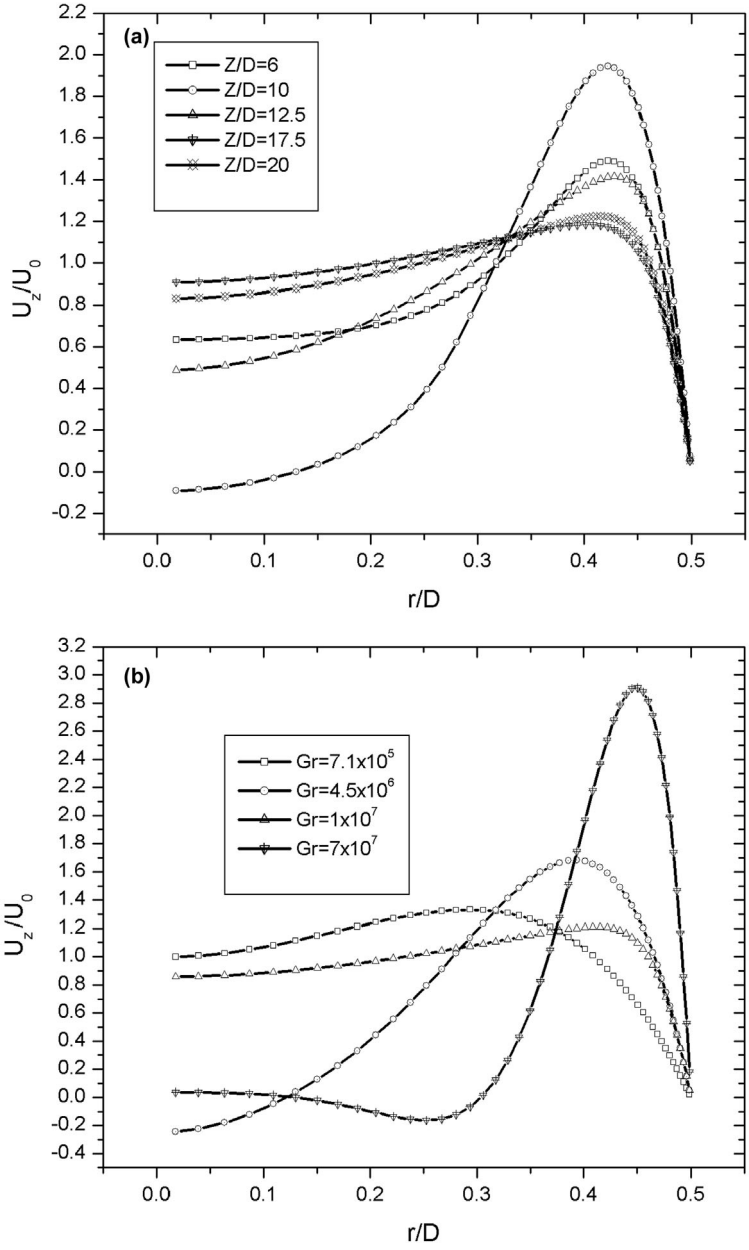

Figure 6.
Axial velocity profiles ($Pr = 0.7$, $Re = 1,000$, $I_0 = 0.1$ percent). (a) Evolution for $Gr = 10^7$ and (b) hydrodynamically developed profiles for different Gr

For $Z/D < 10$ significant velocity variations occur mainly in the vicinity of the wall where the predominating molecular viscosity and the buoyancy induced acceleration counterbalance turbulence production. However, by $Z/D = 10$ an important velocity gradient occurs further away from the wall and gives rise to significant turbulence production and diffusion. These phenomena explain the corresponding sharp increase of k_c shown in Figure 5. The presence of this intense turbulence promotes radial momentum transfer and the velocity profile becomes more uniform as the fluid moves further downstream. Therefore, the velocity gradient decreases, turbulence production and diffusion are reduced and by $Z/D = 20$ the velocity profile reaches a form which does not vary much in either the axial or the radial directions. Beyond this point, equilibrium is attained between turbulence production and destruction, which is illustrated by the constant value of k_c shown in Figure 5.

The results of Figures 4 and 5 (axially independent values of U_c and k_c in the downstream region of the tube) as well as those of Figure 6a (small changes of the velocity profile between $Z/D = 17.5$ and $Z/D = 20$) suggest the existence of a hydrodynamically developed region. This has indeed been confirmed by comparing the velocity profiles for a particular Grashof number at different axial cross-sections beyond the positions where U_c and k_c become constant. Figure 6b shows these fully developed axial velocity profiles. Based on the previous observations, the developed profile for $Gr = 10^7$ is turbulent while those corresponding to the other three Grashof numbers are laminar. The three laminar profiles are in good qualitative agreement with the analytical solution for fully developed laminar mixed convection in a vertical uniformly heated tube (Hallman, 1956). For low Grashof numbers the velocity is positive everywhere and its maximum value occurs away from the tube axis. For higher Grashof numbers the maximum velocity increases and moves further away from the axis while the velocity at the centerline decreases and eventually becomes negative (under these conditions, the velocity is zero at an intermediate point between the axis and the wall). Finally, for very high Grashof numbers the region of negative velocities occurs away from the axis (under these conditions, the velocity is zero at two intermediate points between the axis and the wall). Furthermore, the relation between U_c and Gr suggested by our numerical results for the three laminar cases is as predicted by Hallman: as Gr increases U_c decreases, becomes negative and then starts increasing towards positive values. It should be noted that the first two types of laminar profiles shown in Figure 6b by the results corresponding to the two lower Grashof values have also been predicted by laminar numerical models (Zeldin and Schmidt, 1972; Wang *et al.*, 1994; Nesreddine *et al.*, 1998), while the third type corresponding to $Gr = 7 \times 10^7$ has not been obtained numerically by either laminar or turbulent models as far as we can ascertain. Compared with these three laminar profiles, the turbulent one corresponding to $Gr = 10^7$ is, as expected, more uniform. Its maximum is the lowest while its value at the

centerline does not follow the tendency of the other three profiles since the flow regime is not the same.

Figure 7 shows the evolution of the skin friction coefficient for the previously defined cases. At $Z = 0$ the value of C_f is the same for all Grashof numbers and it decreases initially since natural convection effects do not become effective immediately at the tube entrance. For the lowest Grashof number ($Gr = 7.1 \times 10^5$), C_f reaches a local minimum at approximately $Z/D = 5$, increases slightly and attains a constant value of approximately 0.03 in the hydrodynamically developed region. For $Gr = 4.5 \times 10^6$, C_f increases after the entry region, reaches a local maximum and attains a constant value of approximately 0.07 in the developed region. It is noted that, according to the previous discussion, the developed flow for these two Grashof numbers is laminar. For $Gr = 10^7$, for which the developed flow is turbulent, we note a pronounced peak at approximately $Z/D = 10$ corresponding to the position of minimum U_c (cf. Figure 4) and steeply increasing k_c (cf. Figure 5). In the developed region, the value of C_f for $Gr = 10^7$ is essentially the same as that for $Gr = 4.5 \times 10^6$ despite the fact that the former flow is turbulent while the latter is laminar (cf. Figure 4). Finally, for $Gr = 7.1 \times 10^7$ the values of C_f are much

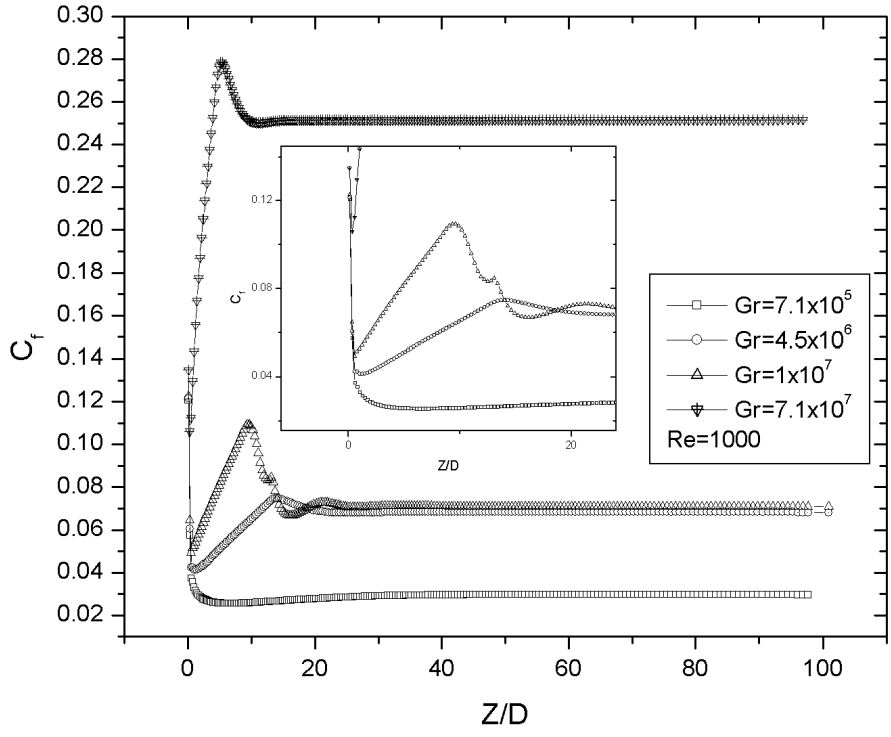

Figure 7.
Evolution of the skin friction coefficient ($Pr = 0.7$, $Re = 1,000$, $I_0 = 0.1$ percent)

higher than those for all previous cases despite the fact that beyond approximately $Z/D = 5$ this flow field is laminar (cf. Figure 5). It should be noted that the value of C_f for hydrodynamically developed forced convection is 0.016, i.e. considerably smaller than all the values shown in Figure 7.

Conclusion

The three-dimensional elliptic conservation equations and the Launder and Sharma low Reynolds number k-ε turbulent model were used to study steady state, developing, ascending mixed convection of air in a uniformly heated vertical tube. The adopted formulation has been successfully validated against experimental results for both laminar and turbulent flow conditions.

A detailed analysis of flow variables calculated for $\mathrm{Re} = 1,000$ and a wide range of Grashof numbers has established the existence of fully developed flow conditions. The corresponding flow regime is laminar for $\mathrm{Gr} < 8 \times 10^6$, turbulent for $8 \times 10^6 < \mathrm{Gr} < 5 \times 10^7$ and again laminar for $\mathrm{Gr} > 5 \times 10^7$. The existence of a laminar velocity profile with flow reversal away from the axis, in accordance with the analytical solution for fully developed flow obtained by Hallman, has been demonstrated numerically.

It has also been shown that for $\mathrm{Re} = 1,000$ and low or high Grashof numbers ($\mathrm{Gr} = 7.1 \times 10^5$ and $\mathrm{Gr} = 7.1 \times 10^7$) the turbulent kinetic energy decays monotonically as the fluid moves downstream from the tube inlet. This situation corresponds to the laminarization of turbulent mixed convection reported in previous studies for $\mathrm{Re} > 2,500$. On the other hand, for intermediate values of the Grashof number ($\mathrm{Gr} = 4.5 \times 10^6$ and $\mathrm{Gr} = 10^7$), the turbulent kinetic energy of the flow exhibits a local maximum considerably higher than both the imposed inlet value and its calculated fully developed value. Therefore, for such values of Gr turbulence production exceeds turbulence destruction in some regions of the tube while in others the opposite is true. This result suggests that a laminar flow entering in a heated tube can become turbulent and then again laminar under the combined effects of the Reynolds stresses and the buoyancy force.

These results provide the first systematic description of the flow regime evolution for mixed convection with a Reynolds number below 2,000.

References

Carr, A.P., Connor, M.A. and Buhr, H.D. (1973), "Velocity, temperature, and turbulence measurements in air flow pipe flow with combined free and forced convection", *ASME J. Heat Transfer*, Vol. 94, pp. 211-23.

Cotton, M.A. and Jackson, J.D. (1990), "Vertical tube air flows in the turbulent mixed convection region calculated using a low-Reynolds-number k-ε model", *Int. J. Heat Mass Transfer*, Vol. 33 No. 2, pp. 275-86.

Ezato, K., Shehata, A.M., Kunugi, T. and McEligot, D.M. (1999), "Numerical prediction of transitional features of turbulent forced gas flows in circular tubes with strong heating", *ASME J. Heat Transfer*, Vol. 121 No. 8, pp. 546-55.

Hall, W.B. and Jackson, J.D. (1969), "Laminarization of a turbulent pipe flow by buoyancy forces", *ASME Paper*, No. 96-HT-55.

Hallman, T.M. (1956), "Combined forced and free-laminar heat transfer in vertical tubes with uniform internal heat generation", *ASME J. Heat Transfer*.

Jackson, J.D., Cotton, M.A. and Axcell, B.P. (1989), "Studies of mixed convection in vertical tubes", *Int. J. Heat Fluid Flow*, Vol. 10 No. 1, pp. 2-15.

Jones, W.P. and Launder, B.E. (1972), "The prediction of laminarization with a two-equation model of turbulence", *J. Heat Mass Transfer*, Vol. 15, pp. 301-14.

Karasu, T. (1995), "Numerical prediction of turbulent flow in circular pipes", *Numerical Methods in Laminar Turbulent Flow, Proc. Ninth Int. Conf.*, Atlanta, Vol. 9, pp. 1329–1339.

Launder, B.E. and Sharma, B.I. (1974), "Application of the energy dissipation model of turbulence to the calculation of flow near a spinning disc", *Lett. Heat Mass Transfer*, Vol. 1, pp. 131-8.

Metais, B. and Eckert, E.R.G. (1964), "Forced mixed, and free convection regimes", *ASME, J. Heat Transfer*, Vol. 86, pp. 295-6.

Nesreddine, H., Galanis, N. and Nguyen, C.T. (1998), "Effects of axial diffusion on laminar heat transfer with low Péclet numbers in the entrance region of thin vertical tubes", *Numercial Heat Transfer, Part A*, Vol. 33, pp. 247-66.

Orfi, J., Galanis, N. and Nguyen, C.T. (1999), "Bifurcation in steady laminar mixed convection flow in uniformly heated inclined tubes", *Int. J. Num. Meth. Heat Fluid Flow*, Vol. 9, pp. 543-67.

Ouzzane, M. and Galanis, N. (1999), "Effets de la conduction pariétale et de la répatition du flux thermique sur la convection mixte près de l'entrée d'une conduite inclinée", *Int. J. Thermal Sciences*, Vol. 38, pp. 622-33.

Satake, S.I., Kunugi, T. and Shehata, A.M. (2000), "Direct numerical simulation for laminarization of turbulent forced gas flows in circular tubes with strong heating", *Int. J. Heat Fluid Flow*, Vol. 21, pp. 526-34.

Tanaka, H., Marugama, S. and Hatano, S. (1987), "Combined forced and natural convection heat transfer for upward flow in a uniformly heated vertical pipe", *Int. J. Heat Mass Transfer*, Vol. 30 No. 1, pp. 165-74.

Torii, S. and Wen-Jei, Y. (2000), "Thermal-Fluid transport phenomena in strongly heated channel flows", *Int. J. Num. Methods Heat Fluid Flow*, Vol. 10 No. 8, pp. 802-23.

Wang, M., Tsuji, T. and Nagano, Y. (1994), "Mixed convection with flow reversal in the thermal entrance region of horizontal and vertical pipes", *Int. J. Heat Mass Transfer*, Vol. 37, pp. 2305-19.

Zeldin, B. and Schmidt, F.W. (1972), "Developing flow with combined forced free convectionin an isothermal vertical tube", *ASME J. Heat Transfer*, Vol. 94, pp. 211-23.